JCB Article

The *Caenorhabditis elegans vab-10* spectraplakin isoforms protect the epidermis against internal and external forces

Julia M. Bosher,[1] Bum-Soo Hahn,[1] Renaud Legouis,[1] Satis Sookhareea,[1] Robby M. Weimer,[2] Anne Gansmuller,[1] Andrew D. Chisholm,[3] Ann M. Rose,[4] Jean-Louis Bessereau,[2] and Michel Labouesse[1]

[1]Institut de Génétique et de Biologie Moléculaire et Cellulaire (IGBMC), CNRS/INSERM/ULP, BP10142, Illkirch Cedex F-67404, France
[2]Ecole Normale Supérieure de Paris, INSERM U 497, 75005 Paris, France
[3]Department of Molecular, Cellular, and Developmental Biology, University of California, Santa Cruz, CA 95064
[4]Department of Medical Genetics, University of British Columbia, Vancouver, British Columbia, Canada V6T 1Z3

Morphogenesis of the *Caenorhabditis elegans* embryo is driven by actin microfilaments in the epidermis and by sarcomeres in body wall muscles. Both tissues are mechanically coupled, most likely through specialized attachment structures called fibrous organelles (FOs) that connect muscles to the cuticle across the epidermis. Here, we report the identification of new mutations in a gene known as *vab-10*, which lead to severe morphogenesis defects, and show that *vab-10* corresponds to the *C. elegans* spectraplakin locus. Our analysis of *vab-10* reveals novel insights into the role of this plakin subfamily. *vab-10* generates isoforms related either to plectin (termed VAB-10A) or to microtubule actin cross-linking factor plakins (termed VAB-10B). Using specific antibodies and mutations, we show that VAB-10A and VAB-10B have distinct distributions and functions in the epidermis. Loss of VAB-10A impairs the integrity of FOs, leading to epidermal detachment from the cuticle and muscles, hence demonstrating that FOs are functionally and molecularly related to hemidesmosomes. We suggest that this isoform protects against forces external to the epidermis. In contrast, lack of VAB-10B leads to increased epidermal thickness during embryonic morphogenesis when epidermal cells change shape. We suggest that this isoform protects cells against tension that builds up within the epidermis.

Introduction

Morphogenesis is the complex set of processes by which a tissue, an organ, or an organism reaches its final form. It involves numerous changes in shape and position of individual cells. These transformations are driven by molecular motors and cell adhesion complexes; they occasionally require a mechanical coupling between adjacent tissues (Schock and Perrimon, 2002).

Motors molding tissues generate forces that can have shearing effects. Thus, it is likely that they are coupled to molecules acting to preserve cell and tissue integrity. The mechanisms that protect cells against mechanical stresses have seldom been investigated in the context of morphogenesis. Their dissection has instead relied primarily on the analysis of human autoimmune or genetic diseases affecting tissue integrity, and on mouse knockout models. Biochemical and genetic studies have outlined the key function played by integrin- and dystrophin-associated adhesion complexes, plakins, and intermediate filaments (IFs;* Fuchs and Cleveland,

J.M. Bosher, B.-S. Hahn, and R. Legouis contributed equally to this paper.

The online version of this article includes supplemental material.

Address correspondence to Michel Labouesse, IGBMC, CNRS/INSERM/ULP, BP10142, CU de Strasbourg, Illkirch Cedex F-67404, France. Tel.: (33) 3-88-65-33-93. Fax: (33) 3-88-65-32-01. E-mail: lmichel@igbmc.u-strasbg.fr

B.-S. Hahn's present address is National Institute of Agricultural Biotechnology, Metabolic Engineering, Division 225, Seodun-Dong, Suwon, 441-707, South Korea.

R. Legouis' present address is CNRS-CGM, Avenue de la Terrasse, 91190 Gif-sur-Yvette, France.

Key words: plakin; cytoskeleton; hemidesmosome; cell adhesion; morphogenesis

*Abbreviations used in this paper: ABD, actin-binding domain; BPAG, bullous pemphigoid antigen; FO, fibrous organelle; GAR, growth-arrest protein 2–related homology; IF, intermediate filament; MCAF, microtubule actin cross-linking factor; MF, microfilament; MT, microtubule; RNAi, RNA interference.

The Journal of Cell Biology

1998; De Arcangelis and Georges-Labouesse, 2000; Spence et al., 2002). In the skin, for instance, the plectin and bullous pemphigoid antigen (BPAG)-e plakins were shown to link the keratin filaments to α6β4-integrin located in hemidesmosomes (Nievers et al., 1999). Mutations in any of these proteins cause skin blistering disorders on tension or outer abrasion (Pulkkinen and Uitto, 1999; McGrath and Eady, 2001).

We are analyzing the molecular basis and the mechanical aspects of morphogenesis using a genetic strategy in *Caenorhabditis elegans*. *C. elegans* embryos elongate more than fourfold along their anterior–posterior axis in the absence of cell division. This process mainly depends on the epidermis surrounding the embryo and the underlying body wall musculature (Chin-Sang and Chisholm, 2000). The initial phase of elongation, which corresponds to a twofold increase in embryonic length, is driven by the contraction of circumferentially oriented actin microfilaments (MFs) causing changes of epidermal cell shapes (Priess and Hirsh, 1986). Mutations affecting proteins that anchor MFs (α-catenin, β-catenin, E-cadherin) or that organize the MF bundles and regulate their contractions (rho kinase, myosin light chain, spectrins) disrupt embryonic elongation (for review see Chin-Sang and Chisholm, 2000). The subsequent phase of elongation requires the activity of muscle cells, which assemble sarcomeres at the plasma membrane facing epidermal cells during the initial phase (Hresko et al., 1994). Genetic analysis has identified most components involved in building a functional sarcomere (Williams and Waterston, 1994; Mackinnon et al., 2002). Mutations in the corresponding genes generally prevent embryonic elongation beyond the twofold stage, resulting in a terminal phenotype termed Pat, for "paralyzed at twofold" (Williams and Waterston, 1994).

The molecular mechanism underlying the mechanical coupling between muscle and epidermal cells is poorly understood. In *C. elegans*, the external cuticle acts as an exoskeleton onto which muscles attach in order to transform their contractions into body movements. These attachments comprise two distinct entities. Within muscle cells, dense bodies at the level of thin filaments and the M-line at the level of thick filaments anchor sarcomeres to the muscle plasma membrane. They are functionally and molecularly related to vertebrate adhesion plaques, including, for instance, an integrin dimer called PAT-2/PAT-3 (Williams and Waterston, 1994; Gettner et al., 1995; Mackinnon et al., 2002). Within epidermal cells, a series of small electron-dense plaques are found at the basal and apical membranes facing muscles and the cuticle, respectively. These plaques are reminiscent of vertebrate hemidesmosomes because they are connected to IFs (Francis and Waterston, 1985). The entire unit (plaques and IFs) is known as a fibrous organelle (FO). Besides IFs, another potential FO component, based on its distribution, corresponds to the uncharacterized protein recognized by the mAb MH5 that was generated by immunizing mice against muscle- and cuticle-associated extracts (Francis and Waterston, 1985, 1991). Molecules that might connect FOs to the ECM and the cuticle include myotactin at the epidermal basal surface, and MUP-4 and MUA-3 at the epidermal apical surface (Hresko et al., 1999; Bercher et al., 2001; Hong et al., 2001). Inactivation of known FO components causes a detachment of muscle cells from the epidermis and/or a detachment of the epidermis from the cuticle, suggesting that FOs are essential to maintain the muscle–cuticle attachment (Hresko et al., 1999; Bercher et al., 2001; Hong et al., 2001; Karabinos et al., 2001).

A screen for mutants with elongation defects led us to characterize a gene known as *vab-10*. We report that *vab-10* corresponds to the *C. elegans* spectraplakin locus, a recently recognized plakin subfamily defined by vertebrate *BPAG1* and *MACF1,* and by *Drosophila shot* loci (Roper et al., 2002). The roles of BPAG1 and microtubule actin cross-linking factor (MACF) 1 during morphogenesis, if any, have not yet been described (Fuchs and Karakesisoglou, 2001; Leung et al., 2002). Shot is known to form complexes with integrins and play a function very similar to that of plectin/BPAG1-e in vertebrate epidermal cells (Gregory and Brown, 1998; Prokop et al., 1998; Strumpf and Volk, 1998). However, besides its role in controlling actin remodeling in tracheal cells, its function during morphogenesis has not been fully investigated (Lee and Kolodziej, 2002a). We show that in *C. elegans*, *vab-10* encodes several protein isoforms related either to plectin and BPAG1-e, or to MACF and BPAG1-a, with distinct functions in the epidermis. Our work shows that molecules initially described for their role in protecting cells against mechanical stress are essential for epithelial and embryonic morphogenesis. We suggest that spectraplakins protect epidermal cells against external forces exerted by muscles, and against internal forces resulting from cell shape changes occurring in the epidermis.

Results

Identification of v*ab-10* alleles

Previously, we performed a genetic screen to identify loci required for embryonic morphogenesis, and reported that embryos homozygous for the chromosomal deficiency *hDf17* arrest with severe morphogenic defects (Labouesse, 1997). We could identify an embryonic lethal mutation, *h1356*, that recapitulates some aspects of the *hDf17* mutant phenotype (Fig. 1 B), and then found that *h1356* is allelic to the viable mutation *vab-10*(*e698*). This allele was originally identified for its variable head morphogenesis defects (*vab*, variably abnormal), and was later observed to cause muscle attachments to be fragile in larvae (Hodgkin, 1983; Plenefisch et al., 2000). In an independent screen for lethal mutants, we identified the *vab-10* allele *ju281* (Fig. 1 C). Finally, after cloning *vab-10*, we recovered the small deletion *mc44* using a molecular approach (Fig. 1 E; see Materials and methods).

vab-10 is a spectraplakin locus that generates two distinct sets of plakins

We molecularly identified *vab-10* by a positional cloning strategy (see Materials and methods). *vab-10* is a complex locus that generates two distinct sets of isoforms by alternative splicing of a common 5′ region to two distinct 3′ regions. The locus spans a region previously predicted to contain three genes (ZK*1151.1*, *ZK1151.2*, and *ZK1151.3*; Fig. 2 A). Using RT-PCR, we identified two distinct sets of isoforms that all contained *ZK1151.1* exons (dark gray) spliced either to *ZK1151.3* (medium gray) or to *ZK1151.2* (light

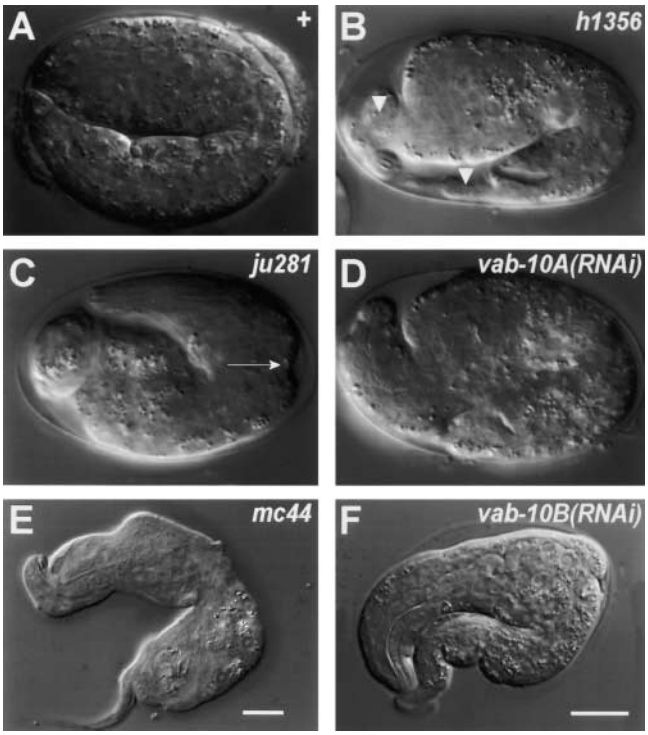

Figure 1. ***vab-10* mutants display elongation and body morphology defects.** Differential interference contrast micrographs of terminal-stage *vab-10* mutants. (A) Wild-type twofold embryo (mid-embryogenesis). (B) *vab-10*(*h1356*) embryo; the body (demarcated by arrowheads) failed to elongate. (C) *vab-10A*(*ju281*) embryo with a localized detachment of the epidermis from the cuticle (arrow); all *vab-10A*(*ju281*) embryos raised at 20°C and 79% of those raised at 25°C ($n = 149$) elongated 2.5-fold like this embryo, and occasionally hatched to generate kinked and paralyzed larvae, whereas 21% of those raised at 25°C looked like *h1356* embryos. (D) *vab-10A*(*RNAi*) embryo; 95% of these embryos ($n = 135$) resembled *h1356* embryos. (E) Arrested L1 *vab-10B*(*mc44*) larva (65%, $n = 403$, could hatch), and (F) hatching L1 *vab-10B*(*RNAi*) larva; the body morphology is very irregular. Embryos laid after eliciting an RNAi response against *vab-10A*– or *vab-10B*–specific exons are denoted *vab-10A*(*RNAi*) or *vab-10B*(*RNAi*). Here (as in Figs. 4, 6, and 8), dorsal is up, anterior is left, and bars represent 10 μm.

gray) exons (Fig. 2 A and Fig. S1, available at http://www.jcb.org/cgi/content/full/jcb.200302151/DC1); these isoforms will subsequently be referred to as *vab-10A* and *vab-10B*, respectively. We identified additional potential splice variants affecting exons 5 and 9 (common region), exon 16 (*vab-10A*–specific exon), and exons 21–23 and 27 (*vab-10B*–specific exons), but could not identify isoforms containing both *ZK1151.3* and *ZK1151.2* exons (Fig. 2 A and Fig. S1). We did not try to determine if all potential combinations of splice variants exist in vivo.

The domains found in the proteins encoded by *vab-10*, its overall sequence similarity with *Drosophila shot*, and their comparable intron/exon organization qualify *vab-10* as the sole *C. elegans* spectraplakin locus (Roper et al., 2002). The common *vab-10* exons code for two potential actin-binding domains (ABD) and a plakin domain; the putative ABD is >50% identical to that of other actin-binding plakins (Andra et al., 1998; Sun et al., 2001; Lee and Kolodziej, 2002b). *vab-10A*–specific exons code for plectin repeats that are preceded by a short coiled-coil rod domain. Comparison with the IF-binding domain of rat plectin (Nikolic et al., 1996) identifies a small region (57% similarity) within the only cluster of five plectin repeats at the COOH terminus of VAB-10A (Fig. S2). This motif cannot be found in any Shot isoform, consistent with the absence of IFs in *Drosophila*. *vab-10B*–specific exons code for spectrin repeats, two EF-hands, and a growth-arrest protein 2–related homology (GAR) domain (Fig. 2 A); there is over 60% identity between the VAB-10B GAR domain and the GAR domain–mediating microtubule (MT) binding in MACF and Shot (Sun et al., 2001; Lee and Kolodziej, 2002b). Compared with vertebrate plakins, VAB-10A is more similar to plectin than to BPAG1-e, and VAB-10B slightly more similar to MACF than to BPAG1-a (Fig. 2 and Fig. S2).

Genetic data validate the molecular model described Fig. 2 A, which predicts that *vab-10A* and *vab-10B* are two distinct transcription units sharing a common 5′ region. The *h1356* mutation affects a splice donor site in the common region and should truncate all isoforms; *e698* and *ju281* are missense mutations affecting *vab-10A* isoforms, and *mc44* is a 1-kb deletion in exons 24–25 that should eliminate the last 1,400 amino acids of VAB-10B isoforms (Fig. 2 A). Consistent with their positions, *h1356* failed to complement the other *vab-10* alleles, whereas *ju281* and *e698* did complement *mc44* (Fig. 2 B). Hereafter, we refer to these alleles as *vab-10*(*h1356*), *vab-10A*(*ju281*), *vab-10A*(*e698*) and *vab-10B*(*mc44*). We suggest that *vab-10*(*h1356*) and *vab-10B*(*mc44*) are very strong or null *vab-10* and *vab-10B* alleles, respectively, as their phenotypes did not become more severe in trans to the deficiency *hDf17*. In contrast, we suggest that *vab-10A*(*ju281*) and *vab-10A*(*e698*) are not *vab-10A* null alleles, as their phenotypes became more severe in trans to *vab-10*(*h1356*) (Fig. 2 B).

VAB-10A and VAB-10B have nonoverlapping distributions in the epidermis

The preceding molecular and genetic data predict that VAB-10A and VAB-10B isoforms should fulfil distinct functions. To address this hypothesis, we set out to examine whether their cellular and subcellular distributions are similar or different. We raised pAbs against one VAB-10A–specific and two VAB-10B–specific domains (Fig. 3). In addition, we used the mAb MH5, known to recognize an FO component (Francis and Waterston, 1991). While characterizing *vab-10*, we noticed that MH5 failed to stain *vab-10*(*h1356*) embryos (Fig. 4 D), suggesting that it might recognize a VAB-10 isoform. Several lines of evidence establish the specificity of these antibodies and demonstrate that MH5 specifically recognizes VAB-10A. First, rabbit polyclonal VAB-10A antibodies detected a band on Western blots that co-migrated with the band detected by MH5 in the 300–400 kD range, in agreement with previous estimates (Francis and Waterston, 1991). Second, VAB-10B antibodies detected a band that migrated above VAB-10A (Fig. 3), consistent with the predicted sizes of both plakins. Third, addition of the polypeptide used to raise the antibodies eliminated the signal recognized by VAB-10A and VAB-10B pAbs (Fig. 3), attesting to their specificity. Last, we could further map the epitope recognized by MH5 within the VAB-10A–specific alternative exon 16 (Fig. S3).

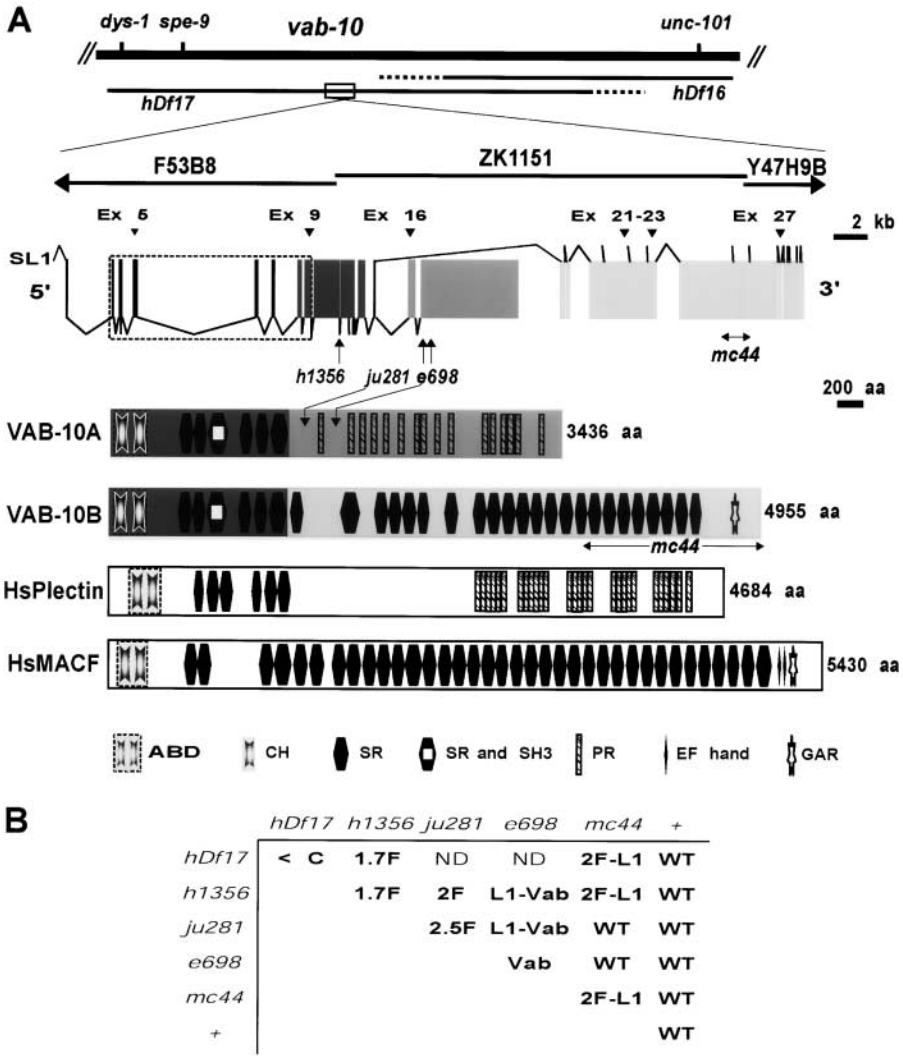

Figure 2. ***vab-10* encodes two distinct plakins.** (A) The first two lines represent the chromosomal region where *vab-10* maps and shows the approximate (dotted areas) endpoints of the deficiencies *hDf17* and *hDf16* used to refine *vab-10* position. *vab-10* spreads over two overlapping cosmids (*F53B8* and *ZK1151*) and a yeast artificial chromosome (*Y47H9B*). The first 15 exons (dark gray boxes, corresponding to a predicted gene known as *ZK1151.1*) are common to *vab-10A* and *vab-10B* isoforms; exons 16–17 (medium gray boxes, corresponding to a predicted gene known as *ZK1151.3*) are unique to *vab-10A* isoforms, exons 18–32 (light gray boxes, corresponding to a predicted gene known as *ZK1151.2*) are unique to *vab-10B* isoforms. Numbered exons (arrowheads) can be alternatively spliced (see Fig. S1). Arrows mark the positions of *vab-10* mutations as follows: *h1356* is a G to A transition in the GT consensus donor splice site of intron 10, leading to a premature stop codon downstream; *ju281* is a G to A transition (nucleotide 20242 of ZK1151) changing the Gly_{1560} of the longest VAB-10A isoform into a Glu; *e698* is a G to A transition (nucleotide 19925 of ZK1151) changing the Pro_{1666} of the longest VAB-10A isoform into a Ser; *mc44* is a 1033-nucleotide deletion (spanning nucleotides 2636–1605 of ZK1151) truncating VAB-10B isoforms after residue 3515. Shown below are the functional domains predicted by the SMART program (http://smart.embl-heidelberg.de) in VAB-10A, VAB-10B, and the two most closely related vertebrate plakins. ABD, actin-binding domain (exons encoding the ABD are surrounded by a dotted box); CH, calponin homology; SH3, Src-homology domain 3; SR, spectrin repeat; PR, plectin repeat; GAR, growth-arrest protein 2-related homology; EF-hand, calcium-binding motif. (B) Complementation tests among *vab-10* alleles bearing on at least 100 individuals of each genotype. Only the most common phenotypes are mentioned (<C, 1.7F, 2F, 2.5F: arrest at the comma, 1.7-fold, twofold, and 2.5-fold stages, respectively; L1: L1 arrest; Vab, variably abnormal; WT, wild-type; ND, not determined).

In embryos, VAB-10A and VAB-10B antibodies first detected a signal at the basal and apical plasma membranes of dorsal and ventral epidermal cells, soon after the onset of differentiation (Fig. 4, A and F). As these cells became thinner during morphogenesis, staining appeared as four longitudinal rows (Fig. 4, B–E and G–L) and progressively evolved into circumferentially oriented bands located above muscle sarcomeres (Fig. 5 A). We also detected VAB-10A basally and apically in the pharynx and along mechanosensory axons as described previously (Francis and Waterston, 1991). VAB-10B was also present in the pharynx lumen, intestine lumen, nerve ring, and in body wall muscles and somatic gonad of larvae (Fig. 4, F–H, and unpublished data; a detailed account of VAB-10 distribution and role in nonepidermal tissues is hoped to be presented elsewhere). These patterns are specific because MH5 and polyclonal VAB-10A antibodies failed to detect a signal in *vab-10*(*h1356*) and *vab-10A*–deficient embryos (Fig. 4, D–E, and Fig. 6 H). Likewise, VAB-10B antibodies could only detect a weak signal in the intestine and pharynx of mid-staged *vab-10B*(*mc44*) and *vab-10*(*h1356*) embryos (Fig. 4, J and L). Although we cannot exclude that VAB-10B antisera recognize a cross-reacting protein, we believe that VAB-10B is expressed in the pharynx and the intestine because surviving *vab-10B*(*mc44*) larvae had an abnormal intestine (unpublished data).

To further define the subcellular level of VAB-10A and VAB-10B in the epidermis, we determined if they colocalize with IFs and myotactin, which are associated with FOs. Using confocal microscopy, we observed that the circumferential bands formed by VAB-10A matched those formed by IFs at all stages (Fig. 5, B/B′). VAB-10A staining strictly colocalized with myotactin in adults (unpublished data), but only partially in young larvae (Fig. 5, C/C′; notice the alternating green and red bands). Reciprocally, we observed that the parallel bands formed by VAB-10B are interspersed with those formed by VAB-10A (Fig. 5, D/D′) and extend beyond the area of muscle–epidermis contact. The VAB-10B

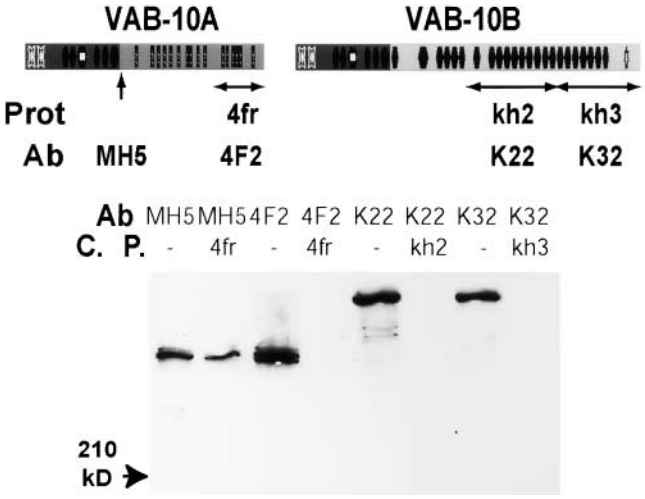

Figure 3. **Characterization of four VAB-10–specific antibodies.** (Top) Positions and names (Prot) of the peptides (horizontal double arrows; domain symbols are as in Fig. 2 A) used to raise antibodies (Ab), and of the epitope recognized by the mAb MH5 (vertical arrow). (Bottom) Western blots of total worm extracts probed with immunopurified antibodies (Ab) in the absence (−) or in the presence of a competing protein (C.P.). Competition with 4fr, kh2, and kh3 recombinant peptides were effective only with the cognate antibodies (e.g., 4fr did not compete interaction with mAb MH5).

bands corresponded to the regularly spaced shallow furrows that pattern the cuticle and separate annuli ridges (Fig. 5, E–E′′; for a description of annuli, see Costa et al., 1997). Immunoelectron microscopy confirmed that VAB-10A (but not VAB-10B) is restricted to FOs. As shown in Fig. 5 (F and G), VAB-10A was exclusively detected in the epidermis in areas dense in filaments, a characteristic of FOs, raising the possibility that VAB-10A might interact with IFs. Using the VAB-10B K22 antibodies, we observed gold particles in the epidermis adjacent to body wall muscles and in sarcomeres (Fig. 5 H). Although the number of particles is low, quantitative analysis indicates that staining is specific (see legend to Fig. 5). Thus, VAB-10B appears to have a disperse distribution in the epidermis and muscles.

VAB-10A is necessary for epidermis attachment to the ECM and VAB-10B to link the apical and basal epidermal plasma membranes

The distinct distributions of VAB-10A and VAB-10B suggest that these isoforms carry out different functions. Consistent with this notion, *vab-10A* and *vab-10B* mutants exhibit different terminal phenotypes. Specifically, embryos with no (or strongly reduced) VAB-10A activity arrested before the two-fold stage of elongation showed no or very little muscle contractions, but had an apparently normal intestine and pharynx (Fig. 1, C and D). *vab-10B*(*mc44*) mutants also failed to elongate beyond the 2.5-fold stage; however, most could hatch (Fig. 1 E) to generate larvae that generally died during the L1 stage with a very irregular and lumpy body morphology. The phenotype of *vab-10B*(*RNAi*) embryos was more variable, but not more severe (Fig. 1 F).

The paralysis of *vab-10A* mutants indicates that muscles are not functional, and the lumpiness of *vab-10B* mutants primarily unveils epidermal defects. Because VAB-10A is as-

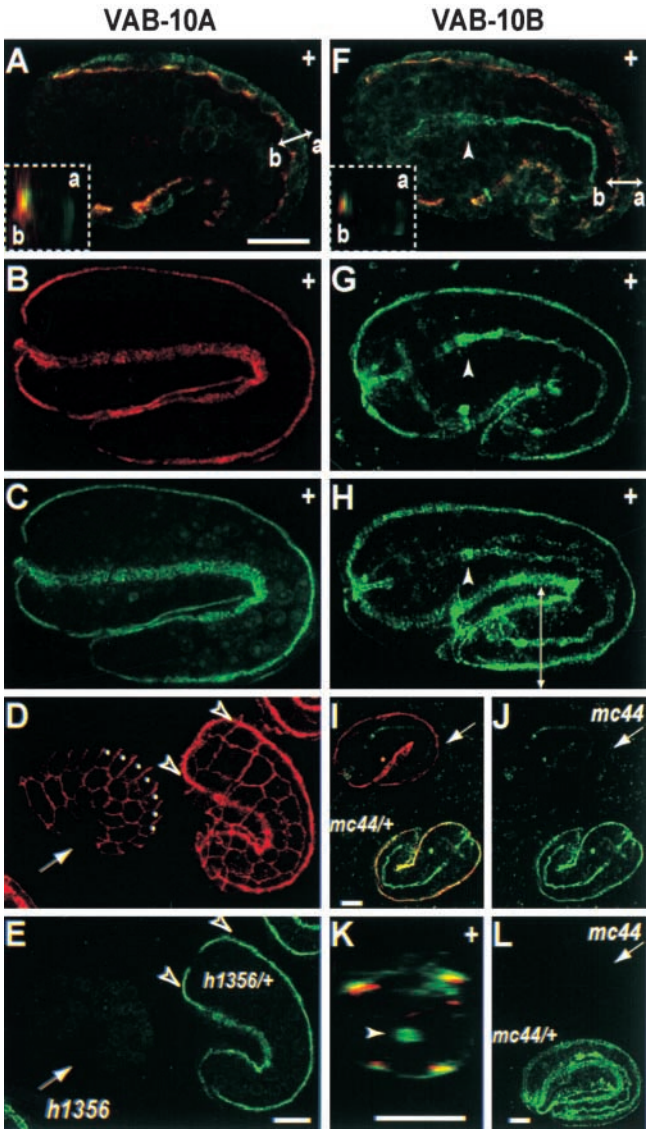

Figure 4. **VAB-10 antibodies recognize regions of epidermis–muscle contact.** Confocal projections of embryos stained with antibodies against VAB-10A (4F2: A, C, and E; MH5: B and D) or VAB-10B (K22: F, G, I, and J; K32: H, K, and L), and with the mAbs MH46 (recognizes myotactin at the basal epidermal membrane in regions of muscle contact; A, F, and I), NE8/4C6 (K, muscle-specific), or MH27 (D, adherens junction-specific; staining with mAbs is in red). (A and F) Early wild-type comma embryos; VAB-10A and VAB-10B staining is detected at the basal (b) and apical (a) membranes as further shown in optical cross sections along the apico–basal axis at the level of arrows (3× insets surrounded by a dotted line). (B and C) Wild-type embryo revealing three muscle–epidermis contact areas. (D and E) *vab-10*(*h1356*) embryo (arrow) and a neighboring heterozygous sibling (right); the VAB-10A signal is absent in the *h1356* mutant embryo even at a stage when muscles are not yet functional (MH27 staining reveals that fusion between dorsal epidermal cells (dots), which normally precedes the first muscle contraction, did not occur yet; arrowheads show two areas of muscle contact in the control). (G and H) Wild-type embryos revealing two muscle–epidermis contact areas, the pharynx and the intestine (arrowhead). (I and J) *vab-10B*(*mc44*) embryo (arrow) and a neighboring heterozygous sibling (bottom); there is a very faint residual staining with K22 antibodies. (K) Z-optical projection through the entire stack of images for the embryo in H at the level of the white bar; VAB-10B is found above muscles (in red) and in the intestine (arrowhead). (L) *vab-10B*(*mc44*) embryo (arrow) and a neighboring heterozygous sibling (bottom); there is essentially no staining with K32 antibodies. Bars, 10 μm.

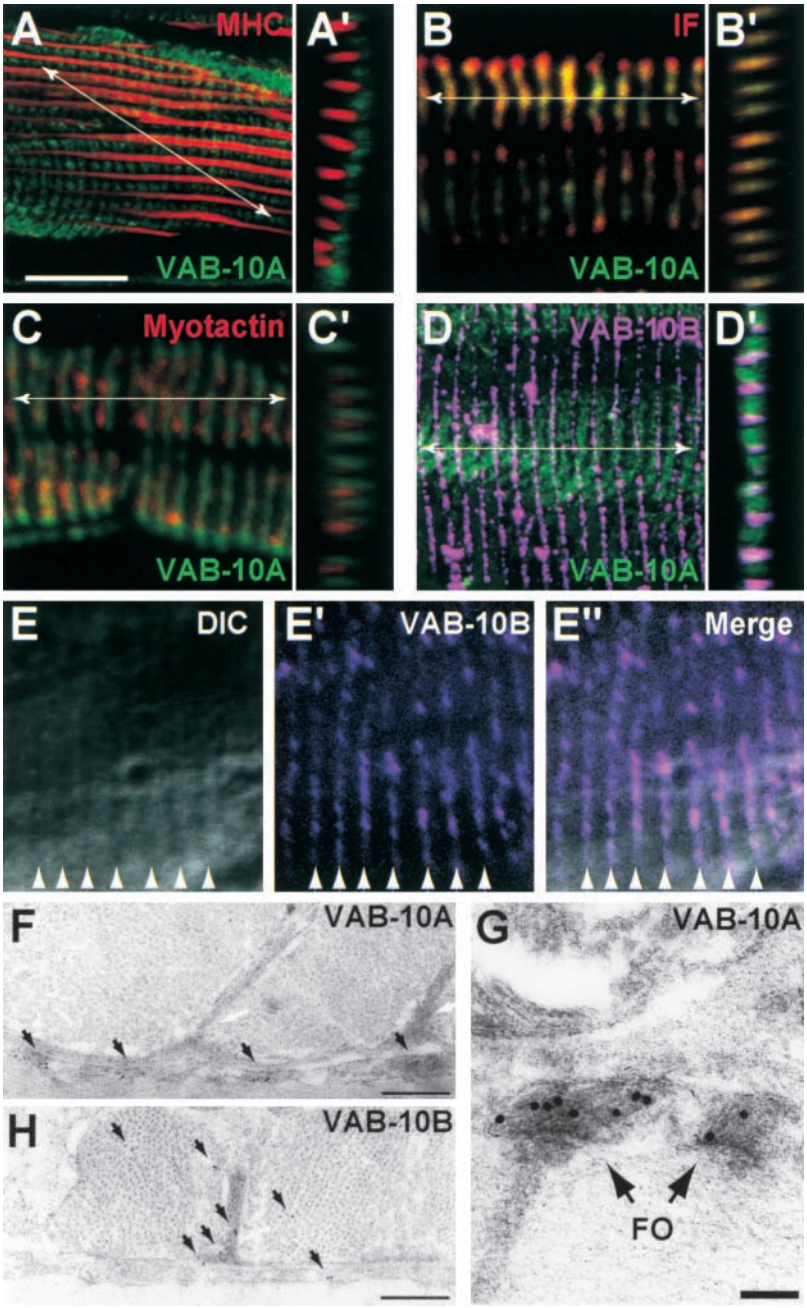

Figure 5. **VAB-10A and VAB-10B form alternating circumferential bands in the larval epidermis.** (Top) Confocal projections (A, B, C, D, and E–E′′), and optical section through the apico–basal axis along the area marked with a double arrow (A′, B′, C′, and D′) after staining wild-type adult animals (A/A′, D/D′, and E′/E′′) or L1 larvae (B/B′ and C/C′); mAb staining is in red. (A/A′) VAB-10A pAbs and myosin heavy chain–specific mAb 5.6.1.1; note the respective orientations (A) and thickness (A′) of sarcomeres and FOs. (B/B′) VAB-10A pAbs (green) and mAb MH4 (IFs; red); both proteins colocalize. (C/C′) VAB-10A pAbs and mAb MH46 (myotactin); these proteins do not generally colocalize. (D/D′) mAb MH5 (VAB-10A; green) and VAB-10B K22 pAbs (violet); these proteins do not colocalize and VAB-10B extends slightly further than VAB-10A. (E–E′′) Differential interference contrast picture (E) of the animal immunostained with VAB-10B K22 pAbs (E′); the merged image (E′′) shows that VAB-10B is found at the furrows separating annuli (arrowheads; due to the permeabilization treatments, their morphology is rather poor). The K32 antiserum revealed the same pattern, but it was much fainter (not depicted). Bar, 10 μm (A and D), 2.5 μm (B and C), or 5 μm (E). (Bottom) Immunogold-labeled micrographs showing the positions of VAB-10A (F and G), and VAB-10B (H) obtained with 4F2 and K22 antibodies, respectively. In the epidermis, VAB-10A (but not VAB-10B) is enriched in FOs (arrowheads, gold particles; white arrows, dense bodies; F and G are from different sections). The specificity of staining is indicated by the signal-to-noise ratio measured by counting gold beads in sections stained with 4F2 or K22 primary antibodies, versus in control sections without primary antibody. 4F2: epidermis, 36.7 ± 4.6, and muscle, 0.9 ± 0.2; K22: epidermis, 4.3 ± 0.5, and muscle, 3.7 ± 0.6 (n = 2). Bars: 500 nm (F and H) and 100 nm (G).

sociated with FOs, which are envisioned as key structures for muscle–epidermis–cuticle attachment, loss of VAB-10A function would be expected to cause the epidermis to detach from the ECM, whereas loss of VAB-10B function should have different consequences. To address this issue, we analyzed *vab-10A* and *vab-10B* mutants by light and electron microscopy.

To examine the morphology of muscles and the epidermis, we visualized these tissues with specific antibodies. We used an mAb against a muscle protein with the same distribution as paramyosin (Schnabel, 1995), and VAB-10A antibodies (in *vab-10B*–deficient embryos) or VAB-10B antibodies (in *vab-10A*–deficient embryos); we also used VAB-10A antibodies to stain *vab-10A*(*ju281*) embryos, as *ju281* does not affect VAB-10A synthesis. In wild-type animals, muscles are closely apposed to the epidermis at early stages of elongation (Fig. 6, A–C). Similarly, we found that in VAB-10A–deficient embryos, the positions and shapes of muscle and epidermal cells were normal until the 1.5-fold stage of elongation (Fig. 6, G–J). However, in *vab-10B*(*RNAi*) (Fig. 6, D–F) and *vab-10B*(*mc44*) (unpublished data), at a stage when muscles are not yet functional, muscle cells were located at an unusually large distance from the edge of the embryo on its dorsal side; in these embryos, VAB-10A was detected at two positions, along muscles and along the edge of the embryo. Because VAB-10A is basal and apical in younger wild-type embryos (Fig. 4 A), we interpret this image to mean that muscles still adhere to the epidermis, but that the thickness of epidermal cells dramatically increased.

As muscles become functional (normally at the 1.7/1.8-fold stages), they remain closely apposed to the epidermis in wild-type embryos (Fig. 6 M). However, in *vab-10*(*h1356*), *vab-10A*(*RNAi*), and the most severely affected *vab-10A*(*ju281*) embryos, they gradually collapsed to a central position (Fig. 6 K) while remaining attached to each other and organized into four enlarged quadrants. We believe that muscle activity is directly responsible for this phenotype because muscles were still found attached in the head and tail regions when muscle activity was blocked by simultaneously inducing RNA interference (RNAi) against *vab-10A* and against *myo-3* (Fig. 6 L), the main myosin heavy chain gene (Williams and Waterston, 1994). In addition, VAB-10A and VAB-10B became mutually dependent for their maintenance in the epidermis. VAB-10A was absent in the bodies of most *vab-10A*(*ju281*) (Fig. 6 N) and *vab-10B*(*mc44*) (Fig. 6 O) embryos where muscles had detached. Similarly, VAB-10B was locally undetectable in some *vab-10A*(*ju281*) embryos mainly in areas where muscles had detached (Fig. 6, P–R, arrows), and was essentially absent at the end of embryogenesis (Fig. 6 K).

The results described (along with Fig. 6) suggest that VAB-10A is essential to anchor muscle cells to the epidermis, and that VAB-10B is required to maintain the distance between the apical and basal plasma membranes of the epidermis. EM analysis allowed us to refine these conclusions. In wild-type embryos, sarcomeres are small relative to larvae and adults, and the dense bodies resemble electron-dense plaques at the plasma membrane instead of the elongated plaques spanning the sarcomeres of larvae and adults (Fig. 7 A). However, in the overlying epidermis,

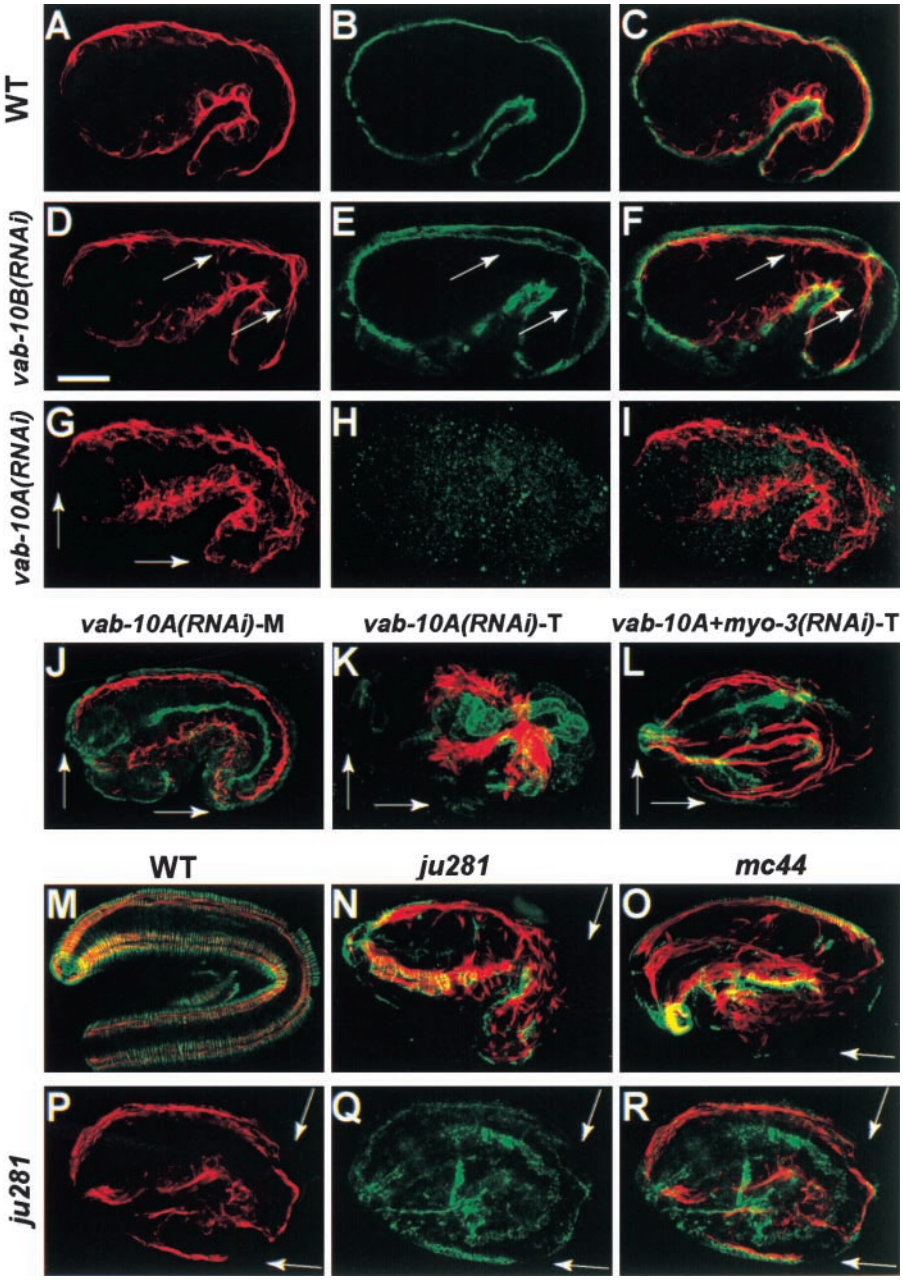

Figure 6. **Integrity and attachment defects in *vab-10* mutants.** Confocal projections after staining mid-stage (A–J and P–R) or terminal-stage embryos (K–O) with the muscle-specific mAb NE8/4C6 (red) and VAB-10A 4F2 antibodies (green; A–I and M–O) or VAB-10B K22 antibodies (green; J–L and P–R); C, F, I, and R correspond to merged images of A and B, D and E, G and H, and P and Q, respectively. (A–C) Wild-type embryo; muscles are adjacent to the epidermis and the outer surface. (D–F) *vab-10B*(*RNAi*) embryo; the epidermal layer is enlarged, although muscles remain adjacent to the basal layer of the epidermis (arrows). (G–K) *vab-10A*(*RNAi*) embryos; muscles always occupied normal positions at mid-embryogenesis extending to the tip of the head and tail (G and J, arrows), but subsequently detached and collapsed to the center of the embryo in 90% of the cases (K, $n = 70$). (L) Simultaneous RNAi against *vab-10A* and *myo-3* (myosin heavy chain gene); muscles remained attached in the head and tail in 74% of the embryos ($n = 69$). (M) Wild-type embryo. (N) *vab-10A*(*ju281*) and (O) *vab-10B*(*mc44*) embryos; VAB-10A is almost absent where muscles have detached (arrows), which occurred in >65% *vab-10B*(*mc44*) embryos and 81% *vab-10A*(*ju281*) embryos ($n > 50$). (P–R) *vab-10A*(*ju281*) embryo; in some areas (arrows) muscles have detached, causing localized loss of VAB-10B staining (a control embryo costained for K32 and NE8/4C6 antibodies is shown in Fig. 4, H and K).

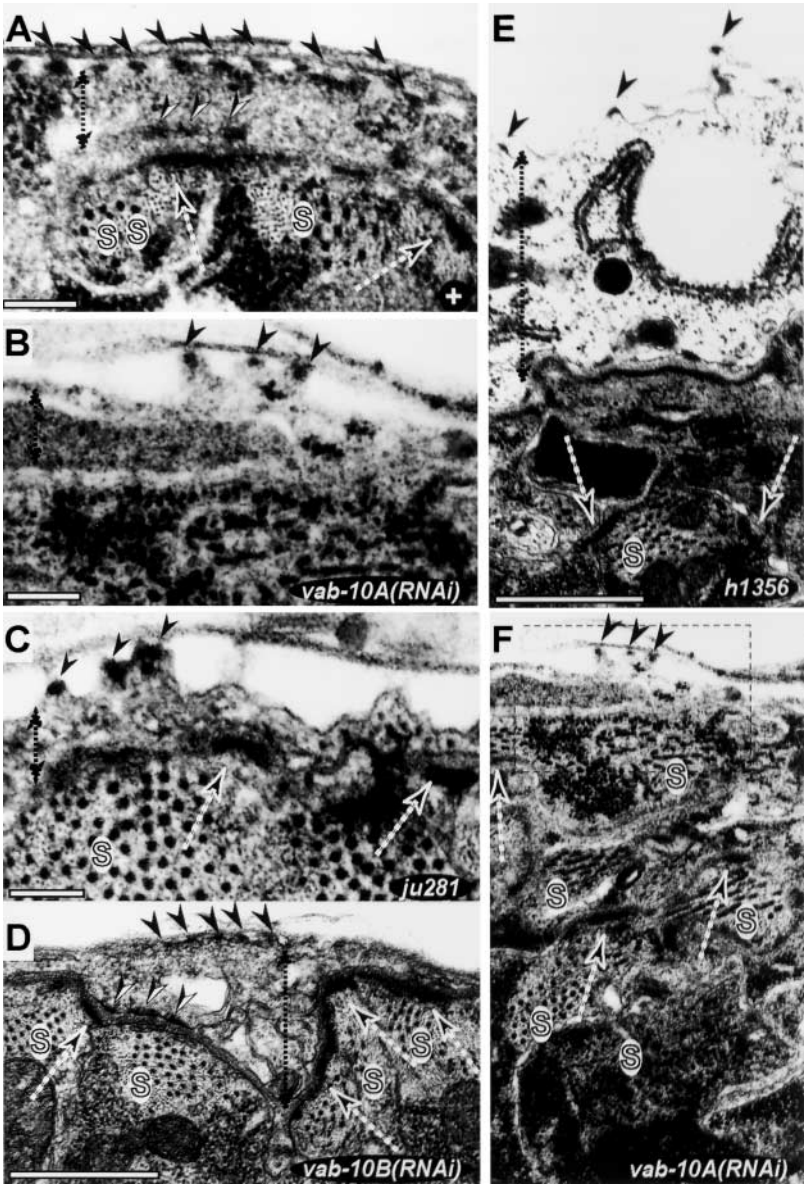

Figure 7. **VAB-10A–deficient mutants have nonfunctional FOs, VAB-10B–deficient mutants have an enlarged epidermis.** EM analysis of cuticle–epidermis–muscle attachments of wild-type (A), *vab-10A*(*RNAi*) (B and F), *vab-10A*(*ju281*) (C), *vab-10B*(*RNAi*) (D), and *vab-10*(*h1356*) (E) embryos. B corresponds to a twofold enlargement of the area boxed in F. Sections are longitudinal to visualize FOs. The wild-type embryo (A) was at a stage when the muscle mass is not yet strongly developed (the fixation procedure used does not allow to visualize IFs). FOs were less numerous and/or not fully functional in VAB-10A–deficient embryos (B, C, and F), but appeared essentially normal in VAB-10B–deficient embryos (D), whereas the epidermal thickness was irregular and significantly increased in VAB-10B–deficient embryos (D); note that *vab-10*(*h1356*) embryos combined both defects (E). Black arrowheads, FO plaque at the apical plasma membrane; semi-open arrowheads, FO plaque at the basal plasma membrane; white open arrows, dense bodies at the muscle plasma membrane; capital S in white oval, sarcomeres; double arrows, epidermal layer. Bars, 1 μm.

FOs had the same appearance as in adults, looking like regularly spaced electron-dense dots found between the developing cuticle or the basal lamina and the epidermis (Fig. 7 A). In *vab-10*(*h1356*) (Fig. 7 E) and *vab-10A*(*RNAi*) (Fig. 7 F), sarcomeres appeared severely disorganized and were not closely apposed to the epidermis. Some greyish material, which probably corresponds to ECM material, accumulated between muscles and the epidermis. Within epidermal cells, we observed fewer FOs than normal in *vab-10A*(*ju281*), *vab-10A*(*RNAi*), and *vab-10*(*h1356*) embryos with gaps between the cuticle and the epidermis (Fig. 7, B, C, and E). One reason why the cuticle–epidermis gap was not wider, except occasionally (Fig. 1 C, arrow), could be that once muscles have pulled away, there is no more tension exerted to widen it. Because we failed to observe similar defects in control embryos, we conclude that VAB-10A is essential to assemble or maintain FOs. In contrast, muscles remained closely apposed to epidermal cells in *vab-10B*(*RNAi*) embryos, but the thickness of epidermal cells was increased even in areas where the number of FOs was normal (Fig. 7 D).

VAB-10A is essential to organize FO components, VAB-10B to strengthen actin filaments

The potential cytoskeleton-binding domains of VAB-10 proteins and the association of VAB-10A with FOs provide some clues as to their functions in epidermal cells. Thus, we examined if these plakins were required for the organization of the cytoskeleton and FO components. Immunostaining with mAbs recognizing IFs and myotactin reveals a regular pattern of circumferentially oriented bands that becomes distinct in wild-type pretzel-staged embryos (Fig. 8, A and C; see also Fig. 5, B and C). However, IFs and myotactin almost never form parallel bands in *vab-10A*(*RNAi*) embryos, except occasionally in the head or the tail, and were generally absent dorsally (Fig. 8, B and D). Ventrally, IFs often collapsed to form thick bundles (Fig. 8 B, arrowheads), which first became apparent at mid-embryogenesis, whereas

myotactin was punctate (Fig. 8 D). These defects, although less severe, were also observed in *vab-10A*(*ju281*)– and VAB-10B–deficient embryos (unpublished data).

Using phalloidin staining, we found that actin MFs could form in *vab-10A*(*RNAi*) embryos and generally had a normal length, but were often not circumferentially oriented (Fig. 8, E and F). In *vab-10B*(*RNAi*) embryos, phalloidin staining was reproducibly fainter, to the point that actin MFs could hardly be detected in some areas (Fig. 8 G). Both types of defects could be seen in *vab-10*(*h1356*) homozygous mutants, in that actin MFs were frequently disorganized and shorter or absent (Fig. 8 H). These data suggest that VAB-10 proteins possess cytoskeleton organizing properties characteristic of plakins.

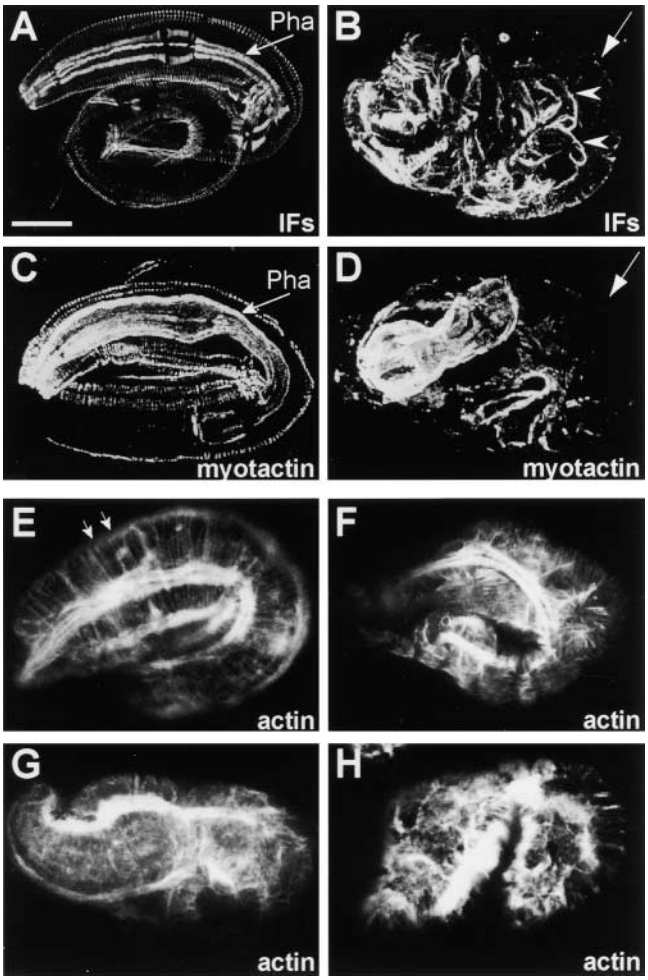

Figure 8. ***vab-10* is required to organize other FO components and actin MFs.** Late-stage embryos were stained with the IF-specific mAb MH4 (A and C), the myotactin-specific mAb MH46 (C and D), or with rhodamine-conjugated phalloidin (E–H). (A and B) Wild-type pretzel embryos; the distributions of IF and myotactin are very similar to what is observed in L1 larvae (see Fig. 5, B and C; both markers are also expressed in the pharynx, see Pha). (B and D) *vab-10A*(*RNAi*) embryo; there is very little IF or myotactin left in the dorsal epidermis (arrow), and IFs tend to bundle together ventrally along what could correspond to lateral membranes (C, arrowheads). (E) Wild-type threefold stage embryo; actin MFs are evenly spaced and oriented along the circumference (arrows). (F) *vab-10A*(*RNAi*) embryo; many actin MFs are irregularly oriented. (G) *vab-10B*(*RNAi*) embryo; actin MFs were reproducibly thin and difficult to visualize. (H) *vab-10*(*h1356*) embryo; actin MFs were short or absent and randomly oriented. Bar, 10 μm.

Discussion

Our data demonstrate that *vab-10* corresponds to the *C. elegans* spectraplakin locus, a plakin subfamily defined by *Drosophila shot* and vertebrate *BPAG1* and *MACF1* loci (Roper et al., 2002). By alternative splicing of a common 5′ region to different sets of 3′ exons, *vab-10* generates two distinct classes of isoforms with essentially nonoverlapping subcellular distributions and different functions in the epidermis. Isoforms related to plectin and BPAG1-e (termed VAB-10A) are essential to maintain the epidermis–ECM attachment. Isoforms related to MACF and BPAG1-a (termed VAB-10B) maintain a connection between the apical and basal epidermal plasma membranes during morphogenesis. A model for VAB-10 distribution and function is presented in Fig. 9 and discussed further in the next paragraph.

vab-10 and other spectraplakin loci

vab-10 shares with other spectraplakin loci the potential to generate a complex set of isoforms, including isoforms with COOH-terminal plectin repeats (VAB-10A) and isoforms with COOH-terminal spectrin repeats (VAB-10B). VAB-10 isoforms possess a potential ABD and VAB-10B a potential microtubule-binding domain, which are well conserved; in contrast, the potential IF-binding domain of VAB-10A isoforms is less well conserved. Future experiments should allow us to test whether these domains are indeed functional. However, our data do not support the existence of a giant *vab-10* transcript similar to BPAG1-b with both central plectin and COOH-terminal spectrin repeats, or imply that such an isoform must be rare and have a minor nonessential function. First, we failed to identify a giant transcript by RT-PCR experiments. Second, VAB-10A and VAB-10B isoforms have different tissue and subcellular distributions, except in the epidermis of early embryos. Finally, *vab-10A* mutations complement *vab-10B* mutations. Our identification of multiple *vab-10* alleles, in an organism that has IFs, provides a more complete genetic analysis of spectraplakin function. In vertebrates, the multiplicity of plakins raises issues of genetic redundancy and complicates the analysis of their protective function during morphogenesis. In *Drosophila*, which has no IFs, previous analyses did not specifically address the function of plectin repeat–containing isoforms (Roper et al., 2002).

FOs are molecularly and functionally homologous to hemidesmosomes

Genetic analysis of *vab-10* mutants strongly suggests that VAB-10A is an essential component of FOs, which have been proposed to mediate muscle–cuticle attachment (Francis and Waterston, 1985). Our data provide the first unambiguous demonstration that FOs are indeed essential to anchor muscles to the cuticle. First, we show by immunoelectron microscopy that VAB-10A is concentrated in FOs. Next, we demonstrate that in the absence of VAB-10A, the number of FOs is reduced, and the epidermis detaches from

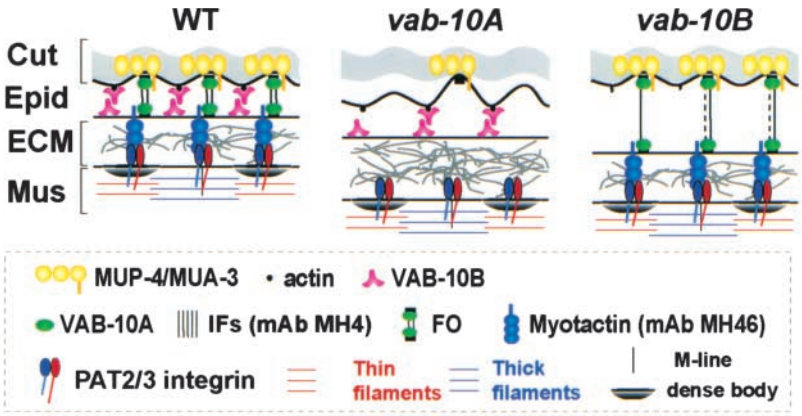

Figure 9. **Model for the distributions and roles of VAB-10 isoforms in the epidermis.** Enlarged view of a muscle–epidermis–cuticle contact area in elongating wild-type (left), *vab-10A* (middle), and *vab-10B* (right) embryos. FOs correspond to the structure formed by electron-dense plaques found at the apical and basal epidermal plasma membranes (black bars) and the interconnecting IFs. Myotactin, MUP-4, and MUA-3 connect FOs to the cuticle (Cut) or the ECM separating the epidermis (Epid) from muscles (Mus). VAB-10A (pink) is an FO component (green), and VAB-10B is interspersed between FOs (pink) and coincides with the furrows separating annuli where actin MFs have also been observed (Costa et al., 1997). Myotactin bands do not fully coincide with VAB-10A bands in young larvae, but do so at later stages. VAB-10B is clearly apical and basal in young embryos, but we do not know if this is also the case later. VAB-10A absence affects FO assembly, causing the epidermis to detach from the ECM and the cuticle. VAB-10B absence causes the epidermal thickness to increase. The molecules that help maintain the distance between apical and basal plasma membranes together with VAB-10B are further discussed in the text. The respective thickness of each layer is not drawn to scale.

the cuticle apically and from muscle cells basally. Finally, we illustrate that a loss of VAB-10A strongly affects the stability of IFs and myotactin, two FO components. Because converse mutations inactivating myotactin (MUA-3 and MUP-4) do not drastically affect IFs or VAB-10A distribution (Hresko et al., 1999; Bercher et al., 2001; Hong et al., 2001), VAB-10A likely acts upstream of these proteins in FO assembly.

FOs have been compared with vertebrate type I hemidesmosomes due to their subcellular position and linkage to IFs. Our analysis establishes that FOs and hemidesmosomes are not only structurally related, but are also functionally and molecularly related. Mutations affecting vertebrate hemidesmosomal components are characterized by a detachment of the epidermis from the ECM (Nievers et al., 1999). Among them, mouse plectin and BPAG1 knockouts lead to the loss of keratin filaments, although they leave some hemidesmosomes intact (Guo et al., 1995; Andra et al., 1997). Likewise, in VAB-10A–deficient embryos, the epidermis is not attached to the ECM, and the stability of IFs is strongly compromised, although some FOs remain visible. The loss-of-function phenotypes of nematode VAB-10A and these mouse plakins are thus similar in these detailed aspects.

Given the considerable evolutionary distance between nematodes and vertebrates, we suggest that a hemidesmosomal-like structure was present in their common ancestor where it probably also mediated resistance to mechanical stress at sites of connection with the ECM. Among vertebrate type I hemidesmosome components (Nievers et al., 1999), plectin appears to be the sole constituent conserved in *C. elegans* (Hutter et al., 2000) because *C. elegans* integrins have not so far been found to be expressed in the epidermis during embryonic elongation (Gettner et al., 1995; Baum and Garriga, 1997). We suggest that a plectin-like protein forms the evolutionarily conserved core component of hemidesmosomal-like structures acting at an early step in the assembly of this ancestral structure.

VAB-10B maintains epidermal integrity

Our results demonstrate that VAB-10B and VAB-10A roles differ. Loss of VAB-10B function leads to increased epidermal thickness at a time when muscle cells are not yet functional, a phenotype that is not observed in VAB-10A–deficient embryos of the same age. This change was visible predominantly on the dorsal side of the embryo, where the epidermis is strongly bent and formed by several cells that fuse at approximately the same time to form a large syncytium called hyp7. Thus, one appealing possibility could be that VAB-10B acts to protect cells against mechanical forces generated within cells that change their shapes. VAB-10B could do so in several ways. For example, *Drosophila* Shot is concentrated at the end of MT bundles in neurons and tendon cells, and is required to anchor these bundles (Gregory and Brown, 1998; Prokop et al., 1998; Lee and Kolodziej, 2002b). By analogy, VAB-10B, which has well conserved actin- and MT-binding domains, could attach to cortical actin and anchor MTs, which are generally oriented along the apico–basal axis in epithelial cells (Fig. 9). An alternative possibility, which takes into account the large size of VAB-10B (4950 aa), the thinness of the epidermis in muscle contact areas (200 nm in early embryos and 50 nm in later embryos), and plakin potential to form dimers through their rod domains (Leung et al., 2002), is that VAB-10B molecules located on the basal and apical membranes dimerize to maintain epidermal thickness (Fig. 9).

Localized change of epidermal thickness might explain why muscles also detach from the epidermis in VAB-10B–deficient embryos. IFs might be unable to maintain a connection between FO plaques when the epidermal thickness increases. In addition, as muscle cells are known to help maintain FOs in the adjacent epidermis (Hresko et al., 1999), perhaps localized weakening of FO integrity triggers a chain reaction, whereby muscle partially detaches, causing further FO instability and increased muscle detachment.

Organization of the cytoskeleton

The mechanism that controls the formation of alternating VAB-10A and VAB-10B circumferential bands is intriguing. The fact that both VAB-10B and actin filament bundles are localized at furrows separating annuli, and the observation that the actin cytoskeleton is perturbed in VAB-10B–deficient embryos, suggest that VAB-10B could play a key role in the initial events that organize VAB-10 and actin distri-

bution. Because VAB-10A and VAB-10B are mutually dependent on each other for their stabilization, the establishment of the alternating pattern of VAB-10B with VAB-10A could be governed by rules of self-organization as often observed for the cytoskeleton (for a discussion on self-organization, see Misteli, 2001).

Elongation of the *C. elegans* embryo depends on the epidermal cytoskeleton and on a communication between muscles and epidermal cells. We have shown that VAB-10 isoforms are essential for embryonic elongation. Future analysis of *vab-10* function should be invaluable to understand how spectraplakins can modulate cytoskeletal dynamics and signaling between tissues during morphogenesis.

Materials and methods

Worm culture and strains

C. elegans strains were grown on NGM plates and fed with OP50 *Escherichia coli* strain at 20°C unless otherwise stated (Brenner, 1974). The allele *vab-10*(*e698*) (Hodgkin, 1983) and the chromosomal deficiency *hDf17* were obtained from the Caenorhabditis Genetics Center (University of Minnesota, Minneapolis, MN).

vab-10 mutations and cloning

The ethyl methane sulfonate–induced lethal mutation *h1356* belongs to a collection of eight lethal mutations isolated in the Rose laboratory (University of British Columbia, Vancouver, Canada). The mutation *ju281* was isolated after ethyl methane sulfonate mutagenesis in screens for larval lethal mutations performed in the Chisholm laboratory (University of California, Santa Cruz, Santa Cruz, CA). We recovered the allele *vab-10*(*mc44*) by PCR screening after trimethylpsoralen/UV mutagenesis using two pairs of nested primers located 2.3 kb apart in *vab-10* exons 23–24 (VAB-10B–specific). One pool carrying a 1-kb deletion (*mc44*), among 96 pools of 25 F1 mutagenized animals, was sib-selected; heterozygous animals segregating *mc44* were outcrossed six times to wild-type animals and balanced. The molecular lesions affecting *vab-10* alleles were identified by sequencing each predicted *vab-10* exon after PCR amplification from *h1356*- and *ju281*-arrested embryos or *e698* adults. Potential mutations were confirmed on an independent embryo/animal. The sequence of *mc44* was determined from *mc44*-arrested larvae. Complementation tests between *vab-10* alleles were performed by crossing *vab-10*(*x*)/+ males with *vab-10*(*y*)/+ hermaphrodites. Mating partners were transferred to fresh plates twice daily, and the number of unhatched eggs, arrested larvae, normal males, and hermaphrodites was counted; retarded larvae (putative trans-heterozygotes) were placed on separate plates and were examined separately.

To molecularly identify *vab-10*, we used RNAi (Fire et al., 1998) against predicted genes mapping under *hDf17* (www.wormbase.org). RNAi against *ZK1151.1*, *ZK1151.2*, and *ZK1151.3*, the three genes predicted within cosmid *ZK1151* (GenBank/EMBL/DDBJ accession no. Z93398), resulted in phenotypes similar or almost identical to those of strong *vab-10* alleles, suggesting that they define a single locus. RT-PCR experiments were performed using the one-step RT-PCR kit (QIAGEN) starting from total RNA (see Fig. S1). The GenBank/EMBL/DDBJ accession nos. for *vab-10* sequences are AJ505815 and AJ505816.

RNAi

Double-stranded RNA (dsRNA) used for RNAi was prepared and injected as described previously (McMahon et al., 2001). RNAi against *vab-10* common exons (positions 25635–26464 of *ZK1151*) generated a phenotype indistinguishable from that of *h1356* mutant embryos. RNAi against *vab-10A*–specific exons was obtained with either of two regions from the large *vab-10A*–specific exon (positions 14630 to 15756, or 19490 and 20417 of *ZK1151*); both dsRNAs produced the phenotypes shown in Fig. 1 E. RNAi against *vab-10B*–specific exons was obtained by co-injecting two dsRNAs from different areas of *vab-10B* (positions 5807 of *Y47H9B* and 518 of *ZK1151*, plus 2018 and 3136 of *ZK1151*). This resulted in *mc44*-like phenotypes within 24–30 h after injection, then phenotypes became weaker; injection of each dsRNA separately resulted in weaker and less penetrant phenotypes.

Generation of VAB-10 antibodies

To produce antibodies, GST fusions with RT-PCR fragments encoding VAB-10A residues G2837–Q3436, VAB-10B residues D2697–R3862, or VAB-10B residues E3863–K4955 were purified using DEAE-Sepharose followed by glutathione-Sepharose 4B columns, and were used to immunize two male New Zealand rabbits. Sera were purified by incubation for 3 h with fusion proteins that had been transferred onto nitrocellulose filters, followed by washing with 0.15 M NaCl for 30 min and PBS for 5 min. Specific antibodies were eluted by 0.1 M glycine-HCl (pH 2.5) for 10 min, and 1 M Tris-HCl (pH 8.0) was added to neutralize the solution. These antibodies were used to detect VAB-10 isoforms (1/1,000 dilution) on Western blots of total worm extracts separated by electrophoresis on 5% acrylamide gels.

Fluorescence microscopy

Embryos were fixed and stained by indirect immunofluorescence or by rhodamine-conjugated phalloidin as described elsewhere (Costa et al., 1997). Primary antibodies were diluted 1:1,000 for VAB-10A– and VAB-10B–immunopurified pAbs, or 1:50 for MH5, MH4, MH46, MH3, MH24, NE8/4C6, and 5.6.1.1 mAbs (Miller et al., 1983; Francis and Waterston, 1991; Schnabel, 1995). MH-series antibodies were a gift from Chelly Hresko and Bob Waterston (Washinton University, St. Louis, MO), NE8/4C6 from the Medical Research Council, and 5.6.1.1 from David Miller (Vanderbilt University, Nashville, TN). Primary antibodies were detected using Cy3- or FITC-conjugated secondary antibodies. Stacks of images every 0.5 μm (0.2 μm for images in Fig. 5 and Fig. 8, E–H) were captured using a confocal microscope (model Sp1; Leica); generally, 12–15 confocal sections were projected using the Tcstk software (McMahon et al., 2001) and then processed using Adobe Photoshop®.

EM

Mutant embryos laid between 6 and 9 h before processing were prepared for EM as described elsewhere (McMahon et al., 2001). Only nonruptured embryos that had reached the 1.5–1.7-fold stage were fixed. Thin sections were examined with a microscope (model EM208; Philips). We examined wild-type or heterozygous mutant/+ background, three embryos and five larvae; *h1356*, four embryos; *ju281*, four embryos; *vab-10A*(*RNAi*) three embryos; and *vab-10B*(*RNAi*), three embryos and six larvae. In each case, at least 10–15 sections at different levels were examined using a 10,000–15,000 magnification.

Immunoelectron microscopy

Wild-type adults were prepared for post-embedded immunolabeling as previously described for studies in other invertebrates (McDonald, 1999). In brief, young adults were immobilized by high pressure freeze, fixed in anhydrous methanol with 4% PFA and 1.5% uranyl acetate at −90°C, and infiltrated at −45°C with lowicryl HM20 (Polyscience, Inc.) that was then polymerized by UV exposure. Thin sections (~80 nm) were incubated with either VAB-10A (1:2,000), VAB-10B K22 (1:500), or no primary antibody, and were labeled with gold colloidal suspensions of a 15-nm diameter coupled to GAR-IgG (BBInternational) according to manufacturer's recommendations (Aurion). Specificity of staining was judged based on comparing the number of gold beads localized in muscle, epidermis, cuticle, and resin in primary antibody–stained and control grids.

Online supplemental material

Fig. S1 presents some of the RT-PCR experiments that lead us to propose the structure of *vab-10* transcripts shown in Fig. 2. Fig. S2 presents, in further details, alignments between the cytoskeleton-binding domains of VAB-10 and other plakins. Fig. S3 describes how we mapped the epitope recognized by the mAb MH5 to *vab-10A* exon 16. Online supplemental material available at http://www.jcb.org/cgi/content/full/jcb.200302151/DC1.

We are indebted to Chelly Hresko for the gifts of MH4, MH5, MH27, and MH46 antibodies. We also thank David Miller and the Medical Research Council for additional antibodies; the Caenorhabditis Genetics Center for strains; Philippe Rostaing, Erik Jorgensen, and Antoine Triller for expert technical assistance with immunoelectron microscopy; the EM facility of IFR 83 for access to the high pressure machine; Jean-Luc Vonesch and Marcel Boeglin for assistance with confocal microscopy; and Elisabeth Georges-Labouesse for critical reading of the manuscript.

J.M. Bosher was supported by fellowships from the Fondation por la Recherche Médicale and the AFM, B.-S. Hahn by the Ministère de la Recherche, and R.M. Weimer by the INSERM "postes verts" program. This work was supported by institutional funds from CNRS, INSERM, Hôpitaux Universitaires de Strasbourg, and grants to M. Labouesse from the Association pour le Recherche sur la Cancer and the EEC-TMR program. Light camera

equipment was purchased with a grant from the Ligue Nationale Centre le Cancer. Work in the laboratory of A.D. Chisholm is supported by a grant from the National Institutes of Health (GM54657)

Submitted: 24 February 2003
Revised: 7 April 2003
Accepted: 10 April 2003

References

Andra, K., H. Lassmann, R. Bittner, S. Shorny, R. Fassler, F. Propst, and G. Wiche. 1997. Targeted inactivation of plectin reveals essential function in maintaining the integrity of skin, muscle, and heart cytoarchitecture. *Genes Dev.* 11:3143–3156.

Andra, K., B. Nikolic, M. Stocher, D. Drenckhahn, and G. Wiche. 1998. Not just scaffolding: plectin regulates actin dynamics in cultured cells. *Genes Dev.* 12: 3442–3451.

Baum, P.D., and G. Garriga. 1997. Neuronal migrations and axon fasciculation are disrupted in *ina-1* integrin mutants. *Neuron.* 19:51–62.

Bercher, M., J. Wahl, B.E. Vogel, C. Lu, E.M. Hedgecock, D.H. Hall, and J.D. Plenefisch. 2001. *mua-3*, a gene required for mechanical tissue integrity in *Caenorhabditis elegans*, encodes a novel transmembrane protein of epithelial attachment complexes. *J. Cell Biol.* 154:415–426.

Brenner, S. 1974. The genetics of *Caenorhabditis elegans. Genetics.* 77:71–94.

Chin-Sang, I.D., and A.D. Chisholm. 2000. Form of the worm: genetics of epidermal morphogenesis in *C. elegans. Trends Genet.* 16:544–551.

Costa, M., B.W. Draper, and J.R. Priess. 1997. The role of actin filaments in patterning the *Caenorhabditis elegans* cuticle. *Dev. Biol.* 184:373–384.

De Arcangelis, A., and E. Georges-Labouesse. 2000. Integrin and ECM functions: roles in vertebrate development. *Trends Genet.* 16:389–395.

Fire, A., S. Xu, M.K. Montgomery, S.A. Kostas, S.E. Driver, and C.C. Mello. 1998. Potent and specific genetic interference by double-stranded RNA in *Caenorhabditis elegans. Nature.* 391:806–811.

Francis, G.R., and R.H. Waterston. 1985. Muscle organization in *Caenorhabditis elegans*: localization of proteins implicated in thin filament attachment and I-band organization. *J. Cell Biol.* 101:1532–1549.

Francis, R., and R.H. Waterston. 1991. Muscle cell attachment in *Caenorhabditis elegans. J. Cell Biol.* 114:465–479.

Fuchs, E., and D.W. Cleveland. 1998. A structural scaffolding of intermediate filaments in health and disease. *Science.* 279:514–519.

Fuchs, E., and I. Karakesisoglou. 2001. Bridging cytoskeletal intersections. *Genes Dev.* 15:1–14.

Gettner, S.N., C. Kenyon, and L.F. Reichardt. 1995. Characterization of beta pat-3 heterodimers, a family of essential integrin receptors in *C. elegans. J. Cell Biol.* 129:1127–1141.

Gregory, S.L., and N.H. Brown. 1998. *kakapo*, a gene required for adhesion between and within cell layers in *Drosophila*, encodes a large cytoskeletal linker protein related to plectin and dystrophin. *J. Cell Biol.* 143:1271–1282.

Guo, L., L. Degenstein, J. Dowling, Q.C. Yu, R. Wollmann, B. Perman, and E. Fuchs. 1995. Gene targeting of BPAG1: abnormalities in mechanical strength and cell migration in stratified epithelia and neurologic degeneration. *Cell.* 81:233–243.

Hodgkin, J.A. 1983. Male phenotypes and mating efficiency in *C. elegans. Genetics.* 103:43–64.

Hong, L., T. Elbl, J. Ward, C. Franzini-Armstrong, K.K. Rybicka, B.K. Gatewood, D.L. Baillie, and E.A. Bucher. 2001. MUP-4 is a novel transmembrane protein with functions in epithelial cell adhesion in *Caenorhabditis elegans. J. Cell Biol.* 154:403–414.

Hresko, M.C., B.D. Williams, and R.H. Waterston. 1994. Assembly of body wall muscle and muscle cell attachment structures in *Caenorhabditis elegans. J. Cell Biol.* 124:491–506.

Hresko, M.C., L.A. Schriefer, P. Shrimankar, and R.H. Waterston. 1999. Myotactin, a novel hypodermal protein involved in muscle-cell adhesion in *Caenorhabditis elegans. J. Cell Biol.* 146:659–672.

Hutter, H., B.E. Vogel, J.D. Plenefisch, C.R. Norris, R.B. Proenca, J. Spieth, C. Guo, S. Mastwal, X. Zhu, J. Scheel, and E.M. Hedgecock. 2000. Conservation and novelty in the evolution of cell adhesion and extracellular matrix genes. *Science.* 287:989–994.

Karabinos, A., H. Schmidt, J. Harborth, R. Schnabel, and K. Weber. 2001. Essential roles for four cytoplasmic intermediate filament proteins in *Caenorhabditis elegans* development. *Proc. Natl. Acad. Sci. USA.* 98:7863–7868.

Labouesse, M. 1997. Deficiency screen based on the monoclonal antibody MH27 to identify genetic loci required for morphogenesis of the *Caenorhabditis elegans* embryo. *Dev. Dyn.* 210:19–32.

Lee, S., and P.A. Kolodziej. 2002a. The plakin Short Stop and the RhoA GTPase are required for E-cadherin-dependent apical surface remodeling during tracheal tube fusion. *Development.* 129:1509–1520.

Lee, S., and P.A. Kolodziej. 2002b. Short Stop provides an essential link between F-actin and microtubules during axon extension. *Development.* 129:1195–1204.

Leung, C.L., K.J. Green, and R.K. Liem. 2002. Plakins: a family of versatile cytolinker proteins. *Trends Cell Biol.* 12:37–45.

Mackinnon, A.C., H. Qadota, K.R. Norman, D.G. Moerman, and B.D. Williams. 2002. *C. elegans* PAT-4/ILK functions as an adaptor protein within integrin adhesion complexes. *Curr. Biol.* 12:787–797.

McDonald, K. 1999. High-pressure freezing for preservation of high resolution fine structure and antigenicity for immunolabeling. *Methods Mol. Biol.* 117: 77–97.

McGrath, J.A., and R.A. Eady. 2001. Recent advances in the molecular basis of inherited skin diseases. *Adv. Genet.* 43:1–32.

McMahon, L., R. Legouis, J.L. Vonesch, and M. Labouesse. 2001. Assembly of *C. elegans* apical junctions involves positioning and compaction by LET-413 and protein aggregation by the MAGUK protein DLG-1. *J. Cell Sci.* 114: 2265–2277.

Miller, D.M. III, I. Ortiz, G.C. Berliner, and H.F. Epstein. 1983. Differential localization of two myosins within nematode thick filaments. *Cell.* 34:477–490.

Misteli, T. 2001. The concept of self-organization in cellular architecture. *J. Cell Biol.* 155:181–185.

Nievers, M.G., R.Q. Schaapveld, and A. Sonnenberg. 1999. Biology and function of hemidesmosomes. *Matrix Biol.* 18:5–17.

Nikolic, B., E. MacNulty, B. Mir, and G. Wiche. 1996. Basic amino acid residue cluster within nuclear targeting sequence motif is essential for cytoplasmic plectin-vimentin network junctions. *J. Cell Biol.* 134:1455–1467.

Plenefisch, J.D., X. Zhu, and E.M. Hedgecock. 2000. Fragile skeletal muscle attachments in dystrophic mutants of *Caenorhabditis elegans*: isolation and characterization of the *mua* genes. *Development.* 127:1197–1207.

Priess, J.R., and D.I. Hirsh. 1986. *Caenorhabditis elegans* morphogenesis: the role of the cytoskeleton in elongation of the embryo. *Dev. Biol.* 117:156–173.

Prokop, A., J. Uhler, J. Roote, and M. Bate. 1998. The *kakapo* mutation affects terminal arborization and central dendritic sprouting of *Drosophila* motorneurons. *J. Cell Biol.* 143:1283–1294.

Pulkkinen, L., and J. Uitto. 1999. Mutation analysis and molecular genetics of epidermolysis bullosa. *Matrix Biol.* 18:29–42.

Roper, K., S.L. Gregory, and N.H. Brown. 2002. The 'Spectraplakins': cytoskeletal giants with characteristics of both spectrin and plakin families. *J. Cell Sci.* 115:4215–4225.

Schnabel, R. 1995. Duels without obvious sense: counteracting inductions involved in body wall muscle development in the *Caenorhabditis elegans* embryo. *Development.* 121:2219–2232.

Schock, F., and N. Perrimon. 2002. Molecular mechanisms of epithelial morphogenesis. *Annu. Rev. Cell Dev. Biol.* 18:463–493.

Spence, H.J., Y.J. Chen, and S.J. Winder. 2002. Muscular dystrophies, the cytoskeleton and cell adhesion. *Bioessays.* 24:542–552.

Strumpf, D., and T. Volk. 1998. Kakapo, a novel cytoskeletal-associated protein is essential for the restricted localization of the neuregulin-like factor, vein, at the muscle-tendon junction site. *J. Cell Biol.* 143:1259–1270.

Sun, D., C.L. Leung, and R.K. Liem. 2001. Characterization of the microtubule binding domain of microtubule actin crosslinking factor (MACF): identification of a novel group of microtubule associated proteins. *J. Cell Sci.* 114: 161–172.

Williams, B.D., and R.H. Waterston. 1994. Genes critical for muscle development and function in *Caenorhabditis elegans* identified through lethal mutations. *J. Cell Biol.* 124:475–490.